


Cite this: *RSC Adv.*, 2019, 9, 36994Received 27th August 2019  
Accepted 22nd October 2019

DOI: 10.1039/c9ra06751e

rsc.li/rsc-advances

# Synthesis, optical, electrochemical properties and anticancer activity of (S)-BINOL cored triazole bridged dendrimers decorated with rhodamine B surface group†

Jothinathan Sathiyar Savithri and Perumal Rajakumar \*

(S)-BINOL cored dendrimers **1–3** with a rhodamine B surface group and triazole bridging unit were synthesized up to second generation in good yield by convergent synthesis through click chemistry. The chiro-optical property of the synthesized dendrimers reveals that the specific rotation increases as the order of dendrimer increases from the zeroth generation to the second generation dendrimer. The electrochemical properties of the dendrimers **1**, **2** and **3** showed quasi-reversible behavior in cyclic voltammetry. The anticancer activity against human hepatocellular carcinoma cell for the second generation dendrimer **3** was found to be better than that for the lower generation dendrimers **1** and **2**.

## Introduction

Chiral dendrimers possess specific properties based on their well-defined highly controlled stereospecific structures, and completely differ from the achiral dendrimers. Chiral dendrimers can achieve important targets due to their unique chiro-optical properties and are therefore used in a wide range of chemical, biological and technological applications. Hence, the synthesis of chiral dendrimers has attracted attention and become an active field of research. Over the last two decades, lots of efforts have been made in the field of the synthesis of a wide range of functionalized dendrimers with unique features to be exploited for different applications in several fields, including catalysis, biology and technology.<sup>1–8</sup>

Chirality is a characteristic feature of many biological systems and plays an important role in the interplay of structure and function. The synthesis of large molecules with chirality offers not only a synthetic challenge for organic chemists but also access to a large spectrum of new molecules. Chiral dendrimers are a class of compounds, which offer the possibility to investigate the impact of chirality in macromolecular systems. The influence of chiral units on supramolecular structures and the application of such structures in areas such as catalysis, biosensor research and optical devices are quite challenging. In order to attain a comprehensive understanding of the chiro-optical properties, well-defined polymers with precise molecular weight and polydispersity are required. In this respect,

dendrimers are excellent candidates for such applications due to their well-defined structure, topology and molecular weight.<sup>9</sup>

Chiral dendrimers are critical in developing highly responsive macromolecular conformational structures that function *via* supramolecular interactions. Chiral dendrimers have potential use in drug delivery, catalysis (including enantioselective catalysis), as catalyst supports, phase transfer catalysts, and as membrane reactors as well as a variety of other applications. (S)-BINOL cored dendrimers show biological activities, such as antibacterial,<sup>10,11</sup> anti-inflammatory,<sup>12</sup> anti-microbial,<sup>13</sup> and anticancer.<sup>14</sup> Thus, the (S)-BINOL unit plays an important role in biology as well as in liquid crystals.<sup>15</sup> Dendrimers with an (S)-BINOL core exhibit interesting chiro-optical and photo-physical properties,<sup>16</sup> and can also be used as entioselective Lewis acid catalysts.<sup>17</sup> Chiral dendrimers with the (S)-BINOL core can be used as a chiral base and chiral auxiliary in organic syntheses.<sup>18</sup> Further, on increasing the dendrimer generation, the dendritic wedges would go farther apart, which could increase the dihedral angle at the naphthyl unit, thereby making them a chiral auxiliary with a higher value of molar rotation. Herein, we report a versatile and highly efficient synthesis and chiro-optical as well as electrochemical properties and anticancer activity of the (S)-BINOL cored dendrimers **1** to **3** (Fig. 1).

## Result and discussion

(S)-BINOL cored rhodamine B decorated triazole bridged dendrimers **1**, **2** and **3** were synthesized *via* a stepwise synthetic methodology. Propargylation, azidation and click reactions were employed to achieve the target chiral triazolyl dendrimers. In order to synthesize the (S)-BINOL cored rhodamine B

Department of Organic Chemistry, University of Madras, Guindy Campus, Chennai – 600 025, Tamil Nadu, India. E-mail: perumalrajakumar@gmail.com; Fax: +91 44 2230 0488; Tel: +91 44 2220 2814

† Electronic supplementary information (ESI) available. See DOI: 10.1039/c9ra06751e



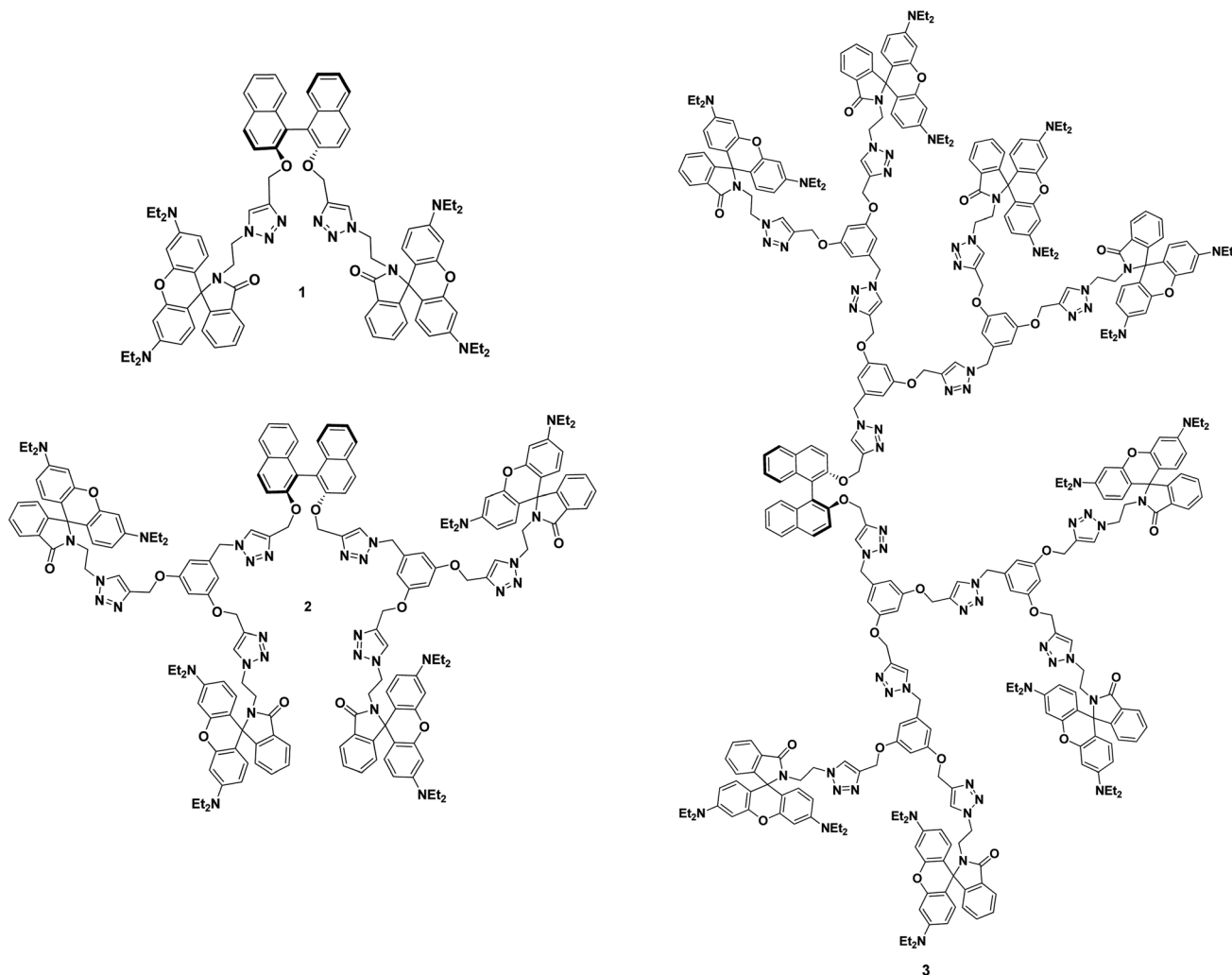


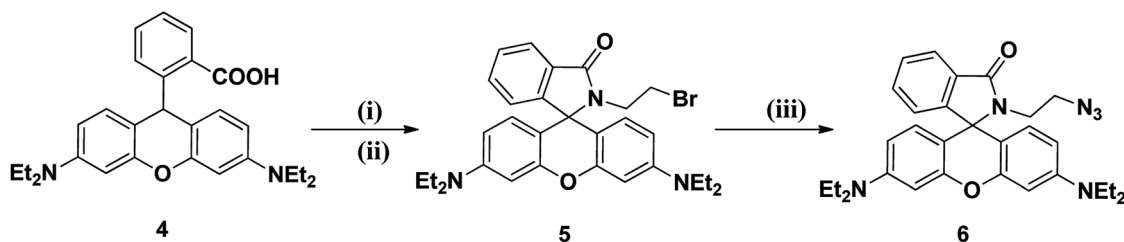
Fig. 1 Molecular structure of (S)-BINOL cored rhodamine B decorated chiral dendrimers 1, 2 and 3.

decorated dendrimers 1, 2 and 3, rhodamine B-capped azido dendrons 6, 9 and 11 were synthesized in good yields using a convergent synthetic route.

In order to explore the utility of rhodamine B as a surface unit in dendrimers, the dendritic wedge 6 was synthesized, as outlined in Scheme 1. The precursor 4 of rhodamine B was refluxed in  $\text{POCl}_3$  for 18 h and concentrated by evaporation, and the rhodamine B acid chloride thus obtained was dissolved in  $\text{CH}_3\text{CN}$ . 2-Bromoethylamine hydrobromide was subsequently

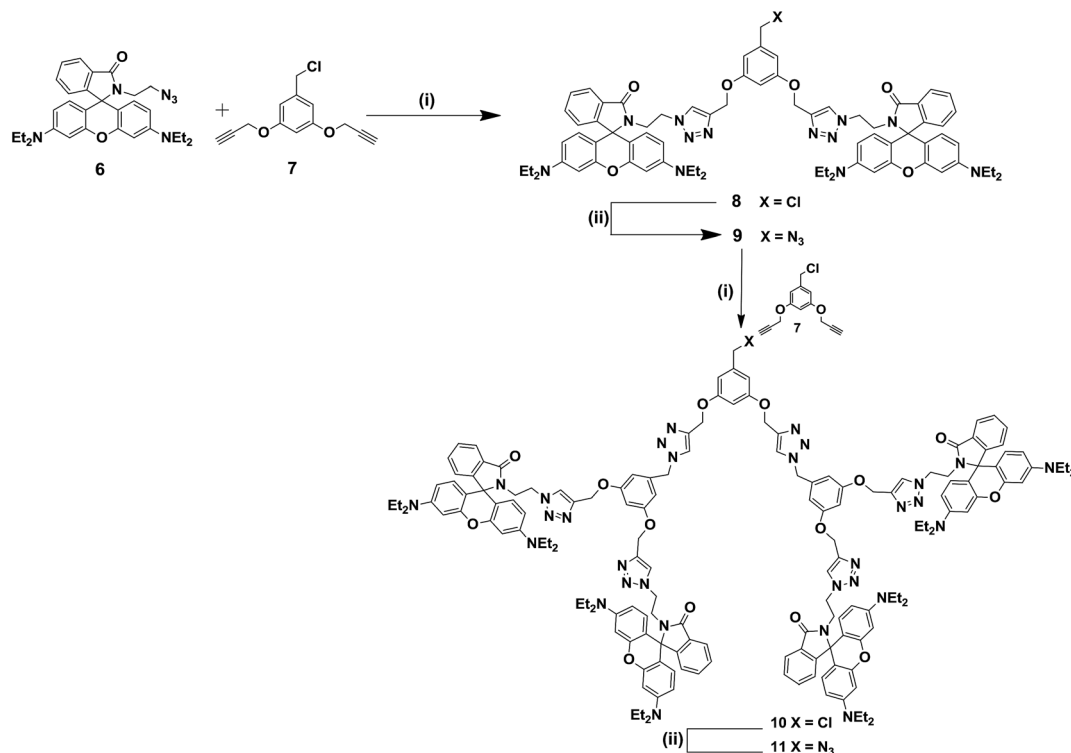
added in the presence of triethylamine and stirred at room temperature for 24 h under  $\text{N}_2$  atmosphere to afford the rhodamine B dendritic bromide 5, which was further reacted with  $\text{NaN}_3$  in a mixture of acetone : water (4 : 1) at 60 °C to yield the rhodamine B azido dendron 6<sup>19</sup> in 95% yield (Scheme 1).

We then focused our attention on the synthesis of precursors for the first and the second generation dendrimers 2 and 3. The synthesis of the first generation dendritic azide 9 is shown in Scheme 2. The reaction of 3,5-bis(propargyloxy)benzyl chloride



Scheme 1 Reagents and conditions: (i)  $\text{POCl}_3$ , 110 °C, 18 h, (ii) 2-bromoethyl amine,  $\text{CH}_3\text{CN}$ , TEA, rt, 24 h, 5 (64%). (iii)  $\text{NaN}_3$ , acetone : water (4 : 1), 60 °C, 10 h, 6 (95%).





**Scheme 2** Reagents and conditions: (i)  $\text{CuSO}_4 \cdot 5\text{H}_2\text{O}$  (5 mol%), sodium ascorbate (10 mol%), THF– $\text{H}_2\text{O}$  (1 : 1), rt, 10 h, **8** (92%), **10** (86%). (ii)  $\text{NaN}_3$ , acetone: water (4 : 1), 60 °C, 10 h, **9** (94%), **11** (92%).

**7** with 2.1 equiv. of rhodamine B azido dendron **6** under Cu(I)-catalyzed click reaction conditions afforded the first generation dendritic chloride **8** in 92% yield, which on further treatment with  $\text{NaN}_3$  in a mixture of acetone/water (4 : 1) at 60 °C for 10 h gave the dendritic azide **9**<sup>19</sup> in 94% yield (Scheme 2). Then, we focused on the synthesis of the second generation dendritic azide **11** from the first generation dendritic azide **9**. The reaction of 1.0 equiv. of 3,5-bis(propargyloxy)benzyl chloride **7** with 2.1 equiv. of the azido dendron **9** under click reaction conditions *viz.*,  $\text{CuSO}_4 \cdot 5\text{H}_2\text{O}$  and sodium ascorbate in a 1 : 1 mixture of THF and water at room temperature afforded the second generation dendritic chloride **10** in 86% yield, which on further treatment with  $\text{NaN}_3$  in a mixture of acetone/water (4 : 1) gave the dendritic azide **11** in 92% yield (Scheme 2).

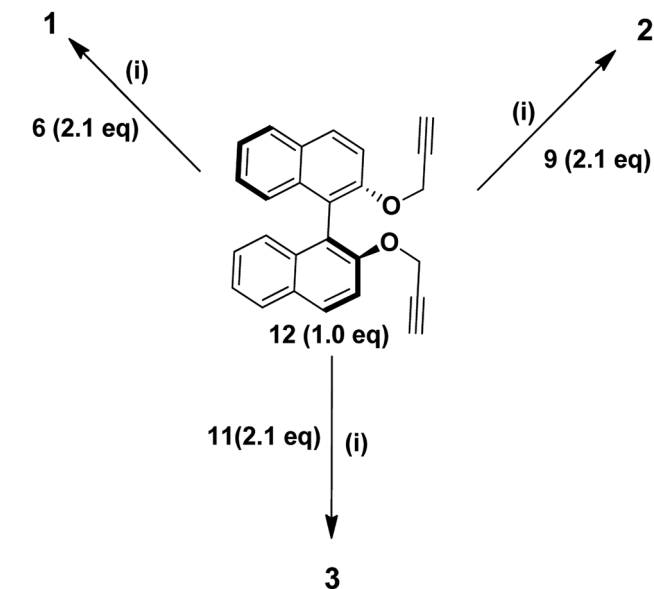
The structure of the dendritic chloride **8** and the dendritic azide **9** was characterized from the spectral and analytical data. The  $^1\text{H}$  NMR spectrum of the second generation dendritic chloride **10** displayed two triplets at  $\delta$  3.59 and 4.16 ppm for the rhodamine *N*-methylene and triazolyl *N*-methylene protons and three singlets at  $\delta$  4.68, 5.03 and 5.40 ppm for the chloro methyl, *O*-methylene and inner triazolyl *N*-methylene protons, respectively, and the triazole protons appeared as singlet at  $\delta$  7.44 ppm and the *N*-ethyl proton at the rhodamine B unit appeared at  $\delta$  1.15 and  $\delta$  3.30 to 3.32 ppm in addition to other aliphatic and aromatic proton signals. The  $^{13}\text{C}$  NMR spectrum of **10** showed the rhodamine *N*-methylene and triazolyl *N*-methylene carbons at  $\delta$  47.8 and  $\delta$  48.2 ppm and signals at  $\delta$  52.0, 62.9,  $\delta$  64.2 ppm for the chloro methyl, inner triazolyl *N*-methylene and *O*-

methylene carbons, respectively. The triazole carbon appeared at  $\delta$  152.4 ppm and rhodamine B carbonyl carbon appeared at  $\delta$  168.3 ppm in addition to the other aliphatic and aromatic carbon signals. Similarly, the structure of the azido dendron **11** was also confirmed from the  $^1\text{H}$  and  $^{13}\text{C}$  spectral and analytical data.

The (S)-BINOL cored rhodamine B decorated dendrimers **1**, **2** and **3** were synthesized regioselectively in 87%, 86% and 78% yields, respectively, by the reaction of 1.0 equiv. of the bispropargyloxy (S)-BINOL core unit **12**<sup>20</sup> with 2.1 equiv. of each of the dendritic azides **6**, **9** and **11** in the presence of  $\text{CuSO}_4 \cdot 5\text{H}_2\text{O}$ , sodium ascorbate in a mixture of THF and water (1 : 1) at room temperature for 12 h, as shown in Scheme 3.

The  $^1\text{H}$  NMR spectrum of the chiral triazole dendrimer **1** showed two triplets at  $\delta$  3.59 and 4.16 ppm for the rhodamine *N*-methylene and triazolyl *N*-methylene protons and a singlet at  $\delta$  5.21 ppm for the *O*-methylene protons, respectively. Another singlet at  $\delta$  7.75 ppm for the triazole protons and the *N*-ethyl proton at the rhodamine B unit appeared as triplet  $\delta$  1.14 for twenty four protons and as quartet  $\delta$  3.32 ppm for sixteen protons in addition to the other aliphatic and aromatic proton signals. The  $^{13}\text{C}$  NMR spectrum of dendrimer **1** displayed signals for the rhodamine *N*-methylene and triazolyl *N*-methylene carbons at  $\delta$  47.8 and  $\delta$  49.2 ppm and the *O*-methylene carbon appeared at  $\delta$  61.8 ppm and the triazole carbon at  $\delta$  153.2 ppm along with the carbonyl carbon at  $\delta$  168.3 ppm in addition to the other aliphatic and aromatic carbon signals. Thus, the structure of the zeroth generation dendrimer **1** was





**Scheme 3** Reagents and conditions: (i)  $\text{CuSO}_4 \cdot 5\text{H}_2\text{O}$  (5 mol%), sodium ascorbate (10 mol%), THF :  $\text{H}_2\text{O}$  (1 : 1), rt, 10 h, **1** (87%), **2** (86%) and **3** (78%).

confirmed from the spectral and analytical data. Similarly, in the  $^1\text{H}$  NMR spectrum of the chiral triazole dendrimer **2**, the *N*-ethyl proton at the rhodamine B unit appeared at  $\delta$  1.12 and  $\delta$  3.30 ppm and the rhodamine *N*-methylene proton and triazolyl *N*-methylene proton appeared as triplet at 3.87 and 4.27 ppm in addition to *O*-methylene and triazolyl proton at 5.10 and 7.61 ppm. The  $^{13}\text{C}$  NMR spectrum of dendrimer **2** exhibited the rhodamine *N*-methylene and triazolyl *N*-methylene carbons at  $\delta$  46.2 and  $\delta$  48.8 ppm and the *O*-methylene carbon appeared at  $\delta$  61.8 ppm. The triazole carbon appeared at  $\delta$  153.4 ppm along with the carbonyl carbon at  $\delta$  168.3 ppm in addition to the other aliphatic and aromatic carbon signals.

Similarly, in the  $^1\text{H}$  NMR spectrum of the chiral triazole dendrimer **3**, the *N*-ethyl proton at the rhodamine B unit appeared at  $\delta$  1.14 and  $\delta$  3.31 ppm and the rhodamine *N*-methylene proton and triazolyl *N*-methylene proton appeared as triplet at 3.81 and 4.60 ppm in addition to *O*-methylene and triazolyl proton at 5.26 and 7.69 ppm. The  $^{13}\text{C}$  NMR spectrum of dendrimer **2** exhibited the rhodamine *N*-methylene and triazolyl *N*-methylene carbons at  $\delta$  47.2 and  $\delta$  53.8 ppm and the *O*-methylene carbon appeared at  $\delta$  62.5 ppm and the triazole carbon at  $\delta$  153.7 ppm along with the carbonyl carbon at  $\delta$  168.5 ppm in addition to the other aliphatic and aromatic carbon signals. Thus, the structure of the first and second generation dendrimers **2** and **3** was confirmed from the spectral and analytical data.

### Chiro-optical property of (S)-BINOL cored rhodamine B decorated dendrimers 1–3

The specific rotation and molar specific rotation values were determined for the (S)-BINOL cored chiral dendrimers **1**, **2** and **3** in DCM at a concentration of  $1 \times 10^{-3}$  M at 589 nm. The specific

**Table 1** Specific and molar rotational values of (S)-BINOL cored dendrimers **1**, **2** and **3**

Dendrimers	Calculated mass	Specific rotation $[\alpha]_{\text{D}}^{25}$	Molar rotation
<b>1</b> (G0)	1383	−18.4	−132.2
<b>2</b> (G1)	2885	−13.5	−161.2
<b>3</b> (G2)	5893	−4.1	−202.7

rotation  $[\alpha]_{\text{D}}^{25}$  and molar rotation values are given in Table 1. The dendrimers **1**, **2**, and **3** can act as chiral auxiliary molecule due to the presence of the (S)-BINOL core unit. The negative specific rotation value decreases with the increase in the dendrimer generation from the zeroth generation **1** (G0) to the second generation dendrimer **3** (G2). The specific rotation value of (S)-BINOL is −35.5. The specific rotation value for the zeroth, first and second generation dendrimers are −18.4, −13.5 and −4.1, respectively. As the bulky nature of the dendritic wedges increases the dihedral angle at the (S)-BINOL unit also increases due to the intramolecular repulsion of the bulky dendritic wedges. The dihedral angle at the (S)-BINOL core increases as the generation of the dendrimer increases to minimize the steric repulsion between the dendritic wedges, thus decreasing the negative value of the specific rotation, which could approach towards the positive side. Herein, the molar rotation value was found to be −132.3 for the zeroth generation dendrimer **1** (G0), 161.2 for the first generation dendrimer **2** (G2) and 202.7 for the second generation dendrimer **3** (G2). Due to increase in the molecular mass, the molar rotation values of the dendrimers **1**, **2** and **3** were found to be −132.2, −161.2, and −202.7, respectively.

### Circular dichroism spectral studies

The circular dichroism spectra were obtained for the zeroth generation dendrimer **1** (G0), the first generation dendrimer **2**

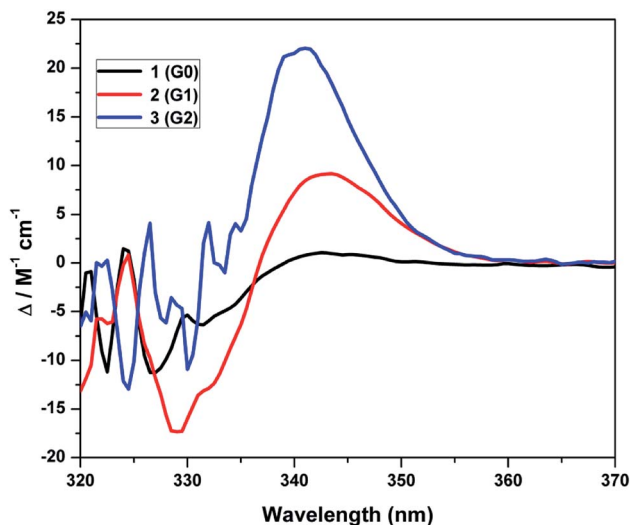


**Fig. 2** Circular dichroism spectra of dendrimers **1–3** at a concentration of 1.0 M in DCM at room temperature.



**Table 2** Circular dichroism spectral data of (S)-BINOL, the zeroth 1 (G0), the first 2 (G1) and the second generation dendrimers 3 (G2)

Dendrimers	Absorbance intensity (nm)	Negative peak ( $M^{-1} cm^{-1}$ )	Absorbance intensity (nm)	Positive peak ( $M^{-1} cm^{-1}$ )
1 (G0)	329	−6.34	342	+1.10
2 (G1)	330	−17.41	342	+8.92
3 (G2)	330	−10.43	342	+22.14

(G2) and the second generation dendrimer 3 (G2) at a concentration of 1.0 M in DCM as solvent (Fig. 2), and the absorbance values are given in Table 2. The circular dichroism spectrum of (S)-BINOL showed a negative peak at 330 nm and a positive peak at 342 nm. The zeroth generation 1 (G0) showed a negative peak at 329 nm with the absorbance intensity of  $-6.34 M^{-1} cm^{-1}$  and the positive signal appeared at 342 nm with the absorbance intensity of  $+1.10 M^{-1} cm^{-1}$ . The first generation dendrimer 2 (G1) showed a negative peak at 330 nm with the absorbance intensity of  $-17.41 M^{-1} cm^{-1}$  and a positive peak appeared at  $+8.90 M^{-1} cm^{-1}$ . Similarly, for the second generation dendrimer 3 (G2), the negative peak appeared at 330 nm with an absorbance intensity of  $-10.43$ . However, the positive peak signal at 342 nm showed the highest intensity of  $+22.14 M^{-1} cm^{-1}$ , which indicate that the dihedral angle at the (S)-BINOL unit increases that results in the highest absorbance intensity of the positive signal as compared with the zeroth generation dendrimer 1 (G0) and the first generation dendrimer 2 (G1). Thus, the circular dichroism spectrum also shows an increase in the dihedral angle at the (S)-BINOL unit when bulky dendritic wedges are attached.

### Photophysical property of (S)-BINOL cored rhodamine B decorated dendrimers 1–3

The absorption and emission spectra of the dendrimers 1, 2 and 3 were recorded in DCM at room temperature. Fig. 3a shows the absorbance spectra of the dendrimers 1, 2 and 3, and the absorbance values are summarized in Table 3. Dendrimer 1, 2 and 3 exhibited three major absorption bands between 478–486,

515–517 and 554–555 nm (Fig. 3), respectively. The absorption band for the rhodamine B unit is usually observed between 540–560 nm absorption bands. The absorption band at 478–486 nm could be due to be  $\pi-\pi^*$  transitions and the absorbance bands at 515–517 and 554–535 nm could be due to the  $n-\pi^*$  transitions from the (S)-BINOL and rhodamine B units. The absorbance intensity increases with the increase in the dendrimer generation from the zeroth generation to the second generation. The zeroth generation dendrimer has only two rhodamine B units. However, the first generation dendrimer and second generation dendrimer have 4 and 8 rhodamine B units, respectively. Hence, on passing from the first generation to the second generation, the intensity of the absorbance band probably increases due to the increase in the number of rhodamine B surface group from 4 to 8 units.

Fig. 3b shows the emission spectra of the (S)-BINOL cored dendrimers 1, 2 and 3 in DCM and the fluorescence parameters are given in Table 3. All the dendrimers exhibited intense fluorescence emission maxima at 575 to 576 nm, on excitation at 520 nm. Upon increasing the number of rhodamine B surface groups, the relative intensity of the emission band also increased from the zero, first and to the second generation dendrimers, which is called the valency effect in dendrimer chemistry.<sup>21</sup> The fluorescence quantum yield ( $\phi_F$ ) of dendrimers 1–3 was measured in DCM using quinine sulphate as the standard. The quantum yields of the dendrimers 1–3 are listed in Table 3. As the generation increases, the quantum yield decreases consistently. The presence of higher number of rhodamine B unit in the second generation dendrimer 3 (G2)

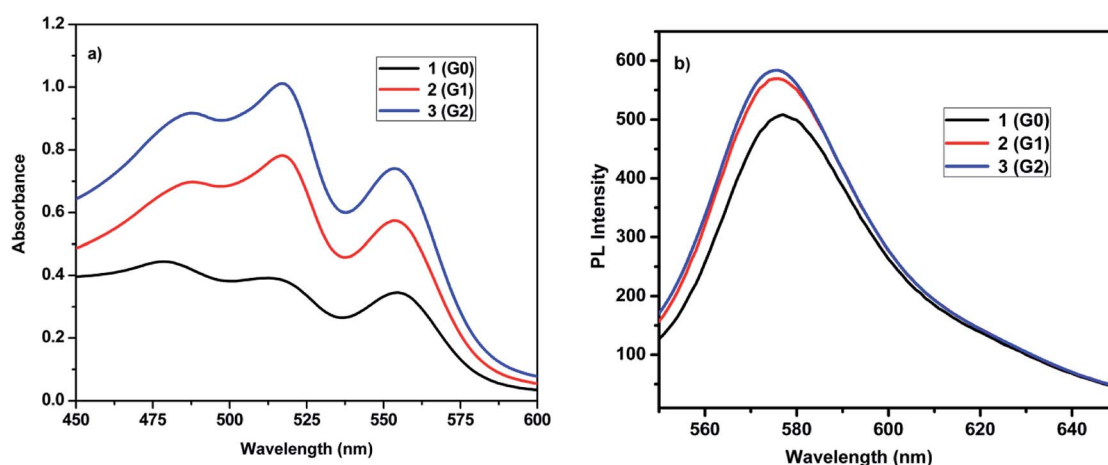


Fig. 3 (a) Absorbance (b) emission spectra of dendrimers 1–3 at a concentration of  $1 \times 10^{-3} M$  in DCM at room temperature.





**Table 3** The absorption, fluorescence data and the electrochemical parameters for the rhodamine B decorated dendrimers **1**, **2** and **3** in DCM ( $1 \times 10^{-5}$  M)

Dendrimers	$\lambda_{\text{abs}}$ max (nm)	Absorption extension coefficient ( $\epsilon \times 10^{-5}$ ) $\text{M}^{-1} \text{cm}^{-1}$	$\lambda_{\text{em}}$ max (nm)	$\phi_{\text{F}}$	$E_{\text{pc}}$	$E_{\text{pa}}$	$\Delta E = E_{\text{pc}} - E_{\text{pa}}$
<b>1</b> (G0)	478, 515, 555	0.44, 0.39, 0.34	576	0.79	−0.42	+0.87	0.45
<b>2</b> (G1)	486, 517, 554	0.69, 0.78, 0.57	575	0.73	−0.46	+0.85	0.39
<b>3</b> (G2)	486, 517, 554	0.96, 1.00, 0.74	575	0.64	−0.41	+0.91	0.50

causes effective fluorescence quenching compared to the lower generation dendrimer **2** (G1) and **1** (G0). As the fluorescence, quenching is efficient in the second generation dendrimer, the quantum yield decreases to 0.64.

### Electrochemical studies of (S)-BINOL cored rhodamine B decorated dendrimers 1–3

The redox behavior of the dendrimers **1**, **2** and **3** was studied by cyclic voltammetry (CV) at room temperature at a scan rate at  $50 \text{ mV s}^{-1}$ . Glassy carbon electrode was used as the working electrode with Pt wire as the counter electrode and Ag/AgCl as the reference electrode. CV studies were carried out for solutions of the substrates (1 mM) in  $\text{CH}_2\text{Cl}_2$  using tetrabutylammonium perchlorate (0.1 M) as the supporting electrolyte. All the as-synthesized dendrimers exhibited electrochemical responses in the cyclic voltammogrammetry, and the cyclic voltammograms of the dendrimers **1**, **2** and **3** are shown in Fig. 4 and the electrochemical parameters are listed in Table 3.

Oxidation and reduction potentials for all the rhodamine B decorated dendrimers **1**, **2** and **3** appeared in the potential range of −0.6 to +1.2 V. The reversible oxidation potential for the rhodamine B decorated dendrimers **1**, **2** and **3** was found to be −0.42, −0.46 and −0.41 V, respectively, and the reversible

reduction peaks were observed at +0.87, +0.85 and +0.91 V for the rhodamine B decorated dendrimers **1**, **2** and **3**, respectively. Negative potential values indicate the presence of more triazole units, which are responsible for the oxidation peak. All the dendrimers showed a high positive potential range of +0.85 to +0.91 V as the extended conjugation of the aromatic rhodamine B moiety requires more energy in the reduction process. Thus, all the as-synthesized dendrimers **1** to **3** showed quasi-reversible behavior in cyclic voltammetry.

### Anticancer activity of (S)-BINOL cored rhodamine B decorated dendrimers 1–3

All the synthesized rhodamine B dendrimers **1**, **2** and **3** were tested for their cytotoxicity against human hepatocellular carcinoma cell line (HUH-7) *via* the MTT assay. In this study, the viability of HUH-7 cells decreased with the increase in the concentrations of the dendrimers, and the data is presented in Table 4 and Fig. 5–8. The therapeutic efficacy of the rhodamine B dendrimers on the inhibition of the growth of hepatocellular carcinoma cell line (HUH-7) was evaluated. The results show that the rhodamine B dendrimers inhibit the growth of cancer cells and the activity was observed to increase along with the increase in the dendritic generation. The presence of the nitrogen and oxygen atoms in the rhodamine B unit enhanced the anticancer activity. The  $\text{IC}_{50}$  value for the rhodamine B dendrimer **3** (G2) was found to be  $15 \mu\text{M}$ , and the  $\text{IC}_{50}$  values for

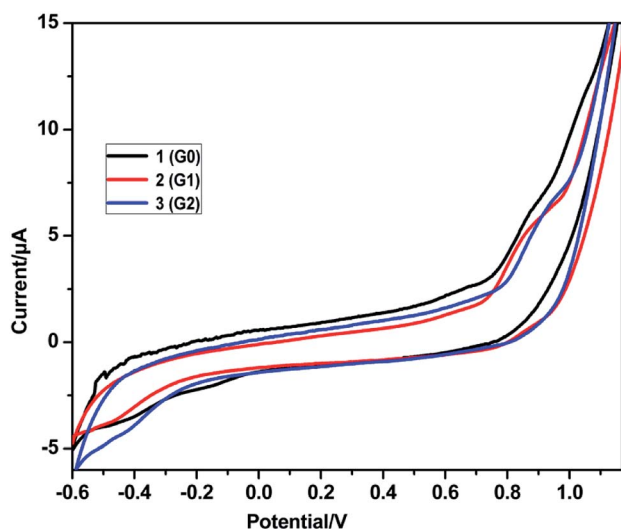


Fig. 4 Cyclic voltammogram of the dendrimers **1**–**3** in  $\text{CH}_2\text{Cl}_2$  ( $1 \times 10^{-3} \text{ mol L}^{-1}$ ), scanned at  $50 \text{ mV s}^{-1}$ .

**Table 4** Inhibition of the cell viability  $\text{IC}_{50}$  value under different concentrations of 5  $\mu\text{M}$ , 10  $\mu\text{M}$ , 15  $\mu\text{M}$ , 20  $\mu\text{M}$ , 25  $\mu\text{M}$ , 50  $\mu\text{M}$  and 100  $\mu\text{M}$  dendrimers **1** (G0), **2** (G1) and **3** (G2) against the growth of the human hepatocellular carcinoma cell line (HUH-7)<sup>a</sup>

Different concentrations of rhodamine B dendrimers <b>1</b> , <b>2</b> , <b>3</b>	Percentage of cell viability (%)		
	<b>1</b> (G0)	<b>2</b> (G1)	<b>3</b> (G2)
Control	100 ± 0	100 ± 0	100 ± 0
5 $\mu\text{M}$	93.9 ± 2.8	88.9 ± 2.6	73.9 ± 2.1
10 $\mu\text{M}$	82.0 ± 2.4	77.0 ± 2.3	61.1 ± 1.7
15 $\mu\text{M}$	75.9 ± 2.2	60.9 ± 1.8	50.3 ± 1.5
20 $\mu\text{M}$	63.0 ± 1.8	50.8 ± 1.9	41.9 ± 1.2
25 $\mu\text{M}$	50.8 ± 1.4	44.8 ± 1.4	34.9 ± 1.0
50 $\mu\text{M}$	42.9 ± 1.2	32.9 ± 0.9	22.1 ± 0.8
100 $\mu\text{M}$	31.8 ± 0.8	23.6 ± 0.4	17.0 ± 0.5
$\text{IC}_{50}$ value	25 $\mu\text{M}$	20 $\mu\text{M}$	15 $\mu\text{M}$

<sup>a</sup> Values are expressed in Mean ± SEM. Each value of mean is triplicate.



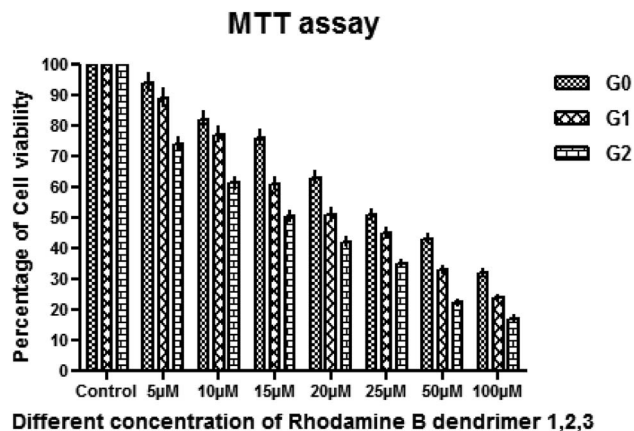


Fig. 5 Anticancer activity at different concentrations of the dendrimers 1 (G0), 2 (G1) and 3 (G2) against human hepatocellular carcinoma cell line (HUH-7).

the lower generation dendrimers 2 (G1) and 1 (G0) were found to be 20  $\mu\text{M}$  and 25  $\mu\text{M}$ , respectively. From the  $\text{IC}_{50}$  values, it is clear that the higher generation dendrimers exhibit better inhibition on the growth of cancer cells than the lower generation dendrimers, which could be due to the higher degree of aggregation in the higher generation dendrimers, as shown by the absorbance and fluorescence studies. Hence, the higher generation rhodamine B dendrimer inhibits the growth of cancer cells to a greater extent than the lower generation dendrimers 1 (G0) and 2 (G1) due to the aggregation effect, as revealed by the photophysical properties. Among the three dendrimers the higher generation dendrimer 3 (G2) inhibits the growth of cancer cells better than the lower generation

dendrimers 1 (G0) and 2 (G1), and the inhibition activity of the three dendrimers is shown in Table 4.

The effect of the concentration of dendrimers 1 (G0), 2 (G1) and 3 (G2) on the inhibition of the growth of cancer cells was further investigated. The concentrations of the dendrimers 1, 2 and 3 at 5  $\mu\text{M}$ , 10  $\mu\text{M}$ , 15  $\mu\text{M}$ , 20  $\mu\text{M}$ , 25  $\mu\text{M}$ , 50  $\mu\text{M}$  and 100  $\mu\text{M}$  were employed for the study. The percentage of inhibition on the growth of cancer cells was found to increase with the increase in the dendrimer concentration. Higher generation dendrimer 3 (G2) at a higher concentration shows better percentage of inhibition on the growth of cancer cells as compared to the lower concentration of the lower generation dendrimers. At a higher concentration of 50  $\mu\text{M}$  and 100  $\mu\text{M}$ , the higher generation dendrimer inhibits the growth of cancer cells better than the lower generation dendrimers at lower concentrations. As the concentration increases, the percentage of inhibition on the growth of cancer cell also increases, which shows that the percentage of inhibition is dose dependant.

## Materials and methods

### Cell line and cell culture

Human hepatocellular carcinoma cell line (Huh-7) was procured from National centre for cell sciences (NCCS), Pune. Huh-7 cells were maintained in T-25 culture flasks and 30 mm Petri dishes, containing Dulbecco's Modified Eagle Medium (DMEM) with 4.5 g  $\text{L}^{-1}$  glucose and L-glutamine (Lonza, USA) supplemented with 10% fetal bovine serum (Himedia) and 1% of antibiotics (100 U  $\text{mL}^{-1}$  penicillin, 100  $\mu\text{g mL}^{-1}$  of streptomycin, 0.25  $\mu\text{g mL}^{-1}$  of amphotericin, Himedia) was incubated in 5%  $\text{CO}_2$  humidified atmosphere at 37  $^{\circ}\text{C}$ .

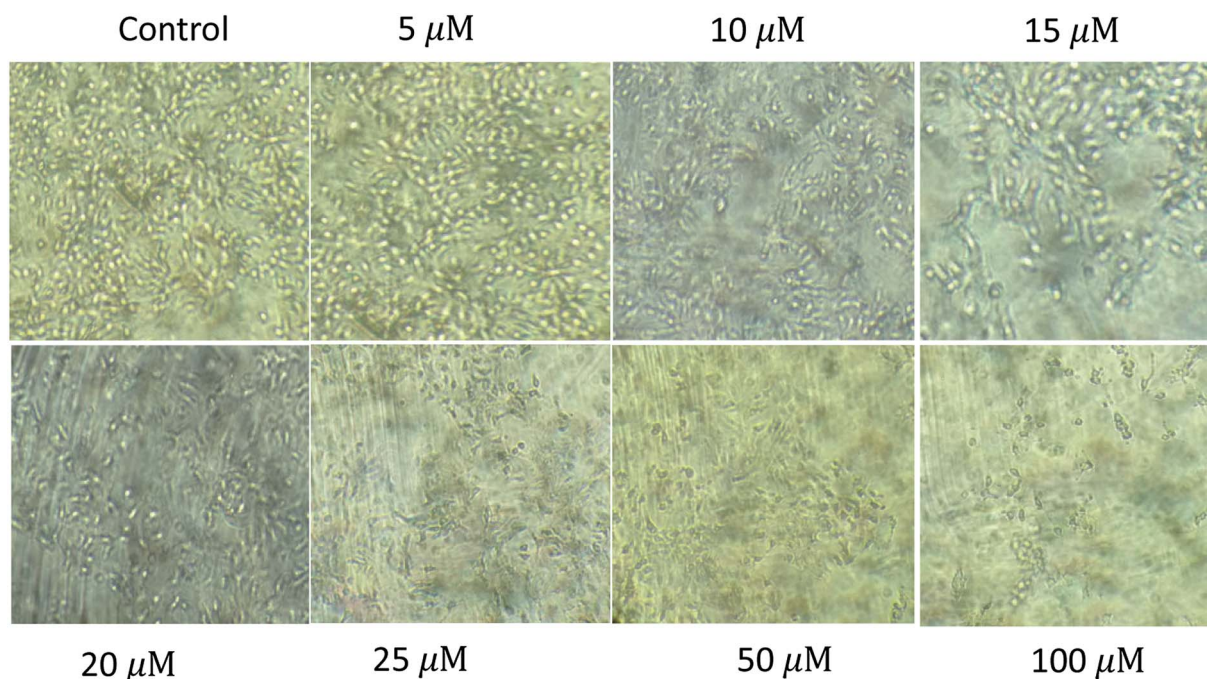


Fig. 6 Cytotoxicity of the zeroth generation dendrimer 1 (G0) on human hepatocellular carcinoma cell line (HUH-7) showing  $\text{IC}_{50}$  at 50  $\mu\text{M}$ .





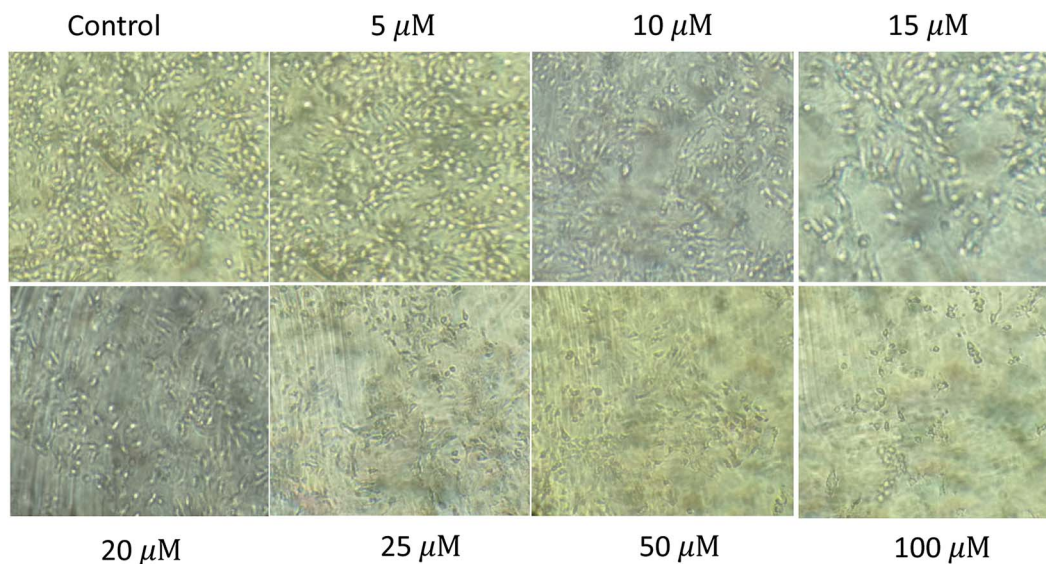


Fig. 7 Cytotoxicity of the first generation dendrimer 2 (G1) on human hepatocellular carcinoma cell line (HUH-7) showing  $IC_{50}$  at 25  $\mu M$ .

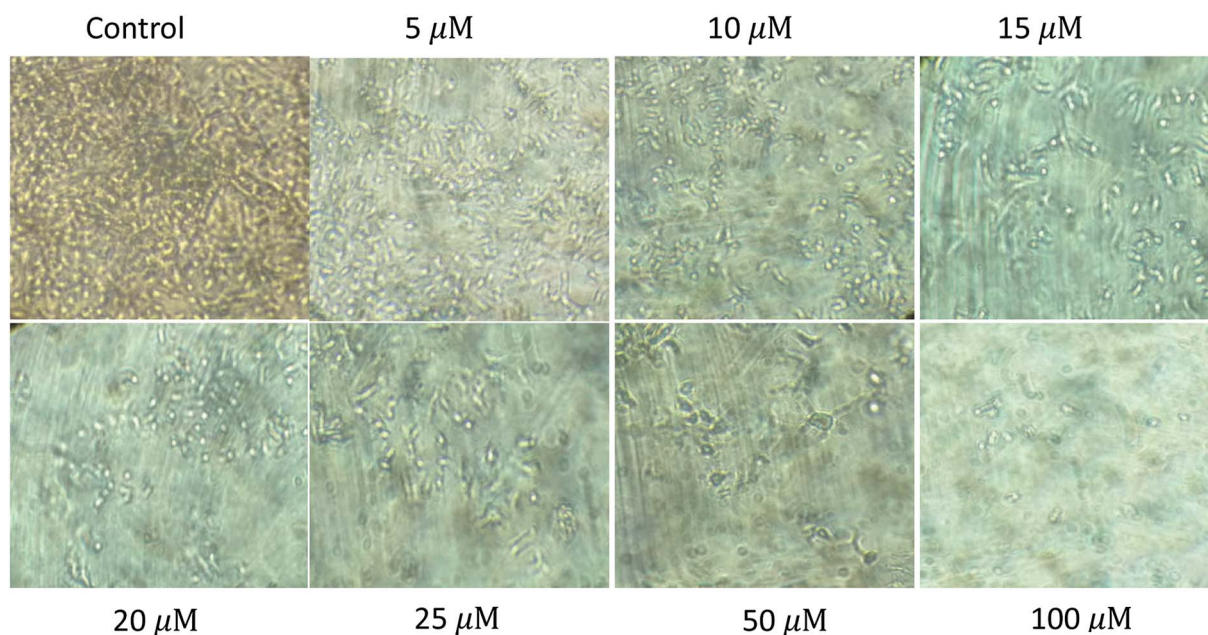


Fig. 8 Cytotoxicity of the second generation dendrimer 3 (G2) on human hepatocellular carcinoma cell line (HUH-7) showing  $IC_{50}$  at 15  $\mu M$ .

#### Cytotoxicity study by MTT assay

Approximately,  $3 \times 10^3$  cells per well were seeded in a 96 well tissue culture plate and the cells were allowed to grow. After 80% of confluency the medium was removed and the cells were treated with various concentrations of rhodamine B, dendrimer 1, 2 and 3 ranging from 5–100  $\mu M$  were incubated for 24 h. After the incubation period, the 10  $\mu L$  of MTT ( $5 \text{ mg mL}^{-1}$ ) was added and again incubated for 4 h at dark at  $37^\circ C$ . The purple colored formazan crystal formed at the bottom was dissolved with 50  $\mu L$  of DMSO for 30 min. The absorbance was recorded at 570 nm on the microplate reader. Percentage of cell viability =  $A_{560 \text{ nm}}$  of treated cells/ $A_{560 \text{ nm}}$  of control cells  $\times 100$ .

#### Morphological study by a phase-contrast microscope

Cells were seeded in six well tissue culture plates on cover slips. After 24 h, the medium was removed and the cells were treated with rhodamine B dendrimers 1, 2 and 3 and incubated for 24 h. After the incubation period, the cells were washed twice with PBS for 5 min and fixed with 400  $\mu L$  of 4% formaldehyde in PBS for 20 min at room temperature. The fixed cells were washed twice with ice cold PBS. The cover slips were gently mounted on the glass slide and the cell morphology was viewed under phase contrast microscope and photographed (Nikon microscope ECLIPSE E400, Japan) at  $10\times$  magnification.





## Conclusion

(S)-BINOL cored rhodamine B decorated triazole bridged dendrimers were successfully synthesized up to second generation *via* click reaction. The photophysical properties of (S)-BINOL cored rhodamine B decorated dendrimers showed that as the generation of the dendrimer increases light absorbing capacity and the intensity of the fluorescence also increases. Similarly, the chiro-optical properties also showed that the specific rotation increases as the dendrimer generation increases, which indicates the widening of the dihedral angle at the (S)-BINOL unit as the bulky nature of the dendritic wedges increase. All the dendrimers show quasi-reversible behavior in cyclic voltammetry. The anticancer activity against human hepatocellular carcinoma cell increases as the dendrimer generation increases from the zeroth to the second generation.

## Conflicts of interest

The authors declare no conflicts of interest.

## Acknowledgements

The authors thank DST-INSPIRE New Delhi, India for financial assistance and DST-FIST for providing NMR facility to the Department of Organic Chemistry, University of Madras, Chennai-25. The authors thank S. Nirmala, Department of biochemistry, University of Madras, Chennai-25 for biological studies. JSS thanks DST-INSPIRE New Delhi for providing fellowship as SRF.

## References

- 1 J. Reek, S. Valo, R. Van Heerbeek, P. Kamer and P. Van Leeuwen, *Adv. Catal.*, 2006, **49**, 71–151.
- 2 H. Crampton and E. Simanek, *Polym. Int.*, 2007, **56**, 489–496.
- 3 D. A. Tomalia, L. Reyna and S. Svenson, *Biochem. Soc. Trans.*, 2007, **35**, 61–67.

- 4 S. Svenson and D. A. Tomalia, *Adv. Drug Delivery Rev.*, 2005, **57**, 2106–2129.
- 5 J. Kofoed and J. L. Reymond, *Curr. Opin. Chem. Biol.*, 2005, **9**, 656–664.
- 6 M. Scholl, Z. Kadlecova and H.-A. Klok, *Prog. Polym. Sci.*, 2009, **34**, 24–61.
- 7 P. R. Dvornic, *J. Polym. Sci., Part A: Polym. Chem.*, 2006, **44**, 2755–2773.
- 8 M. Fischer and F. Vogtle, *Angew. Chem., Int. Ed.*, 1999, **38**, 884–905.
- 9 W. Stadlbauer, *Sci. Synth.*, 2002, **12**, 227–324.
- 10 P. Rajakumar, S. Selvam, V. Shanmugaiah and N. Mathivanan, *Bioorg. Med. Chem. Lett.*, 2007, **15**, 5270–5273.
- 11 A. Thirunarayanan, S. Raja, G. Mohanraj and P. Rajakumar, *RSC Adv.*, 2014, **4**, 41778–41783.
- 12 R. Anandhan, A. Kannan and P. Rajakumar, *Synth. Commun.*, 2017, **47**, 671–679.
- 13 M. Jayanthi and P. Rajakumar, *Int. j. eng. sci. invention res. dev.*, 2016, **3**, 125–133.
- 14 K. Zhang, C. Zhang, Z.-H. He, J. Huang, X. Du, L. Wang and Q. Wang, *ChemBioChem*, 2018, **19**, 2293–2299.
- 15 P. Rajakumar, R. Anandhan and V. Kalpana, *Synlett*, 2009, **9**, 1417–1422.
- 16 L. Ma, S. J. Lee and W. Lin, *Macromolecules*, 2002, **35**, 6178–6184.
- 17 G.-H. Liu, Q.-H. Fan, X.-Q. Yang and X.-M. Chen, *Arkivoc*, 2003, 123.
- 18 (a) A. K. Bandyopadhyaya, N. M. Sangeetha and U. Maitra, *J. Org. Chem.*, 2000, **65**, 8239; (b) L. Pu, *Chem. Rev.*, 1998, **98**, 2405.
- 19 P. Rajakumar and J. Sathiya Savithri, *New J. Chem.*, 2018, **42**, 19390–19399.
- 20 P. Rajakumar and K. Ganesan, *Tetrahedron: Asymmetry*, 2005, **16**, 2295–2298.
- 21 S. Galeazzi, T. M. Hermans, M. Paolino, M. Anzini, L. Mennuni, A. Giordani, G. Caselli and F. Makovee, *Biomacromolecules*, 2010, **11**, 182.

